Branching probe beams by fractional vortex dipoles: Guiding vs. anti-guiding

G. Maleshkov[1], P. Hansinger[2], N. Dimitrov[1], A. Dreischuh[1], G. G. Paulus[2]

[1]Department of Quantum Electronics, Faculty of Physics, Sofia University, Sofia, Bulgaria
[2]Institute of Optics and Quantum Electronics, Faculty of Physics and Astronomy, Friedrich-Schiller-University, Jena, Germany

ABSTRACT

In this work we study the evolution and interaction of semi-infinite dark beams carrying edge-screw phase dislocations in self-focusing and self-defocusing local Kerr nonlinear media aiming to find appropriate conditions to control the process of fusion/crossing the dark beams in a way suitable for probe-beam cross-switching. We show that a quasi-infinite vortex dipole (dipole much longer than the background beam) evolves in a one-dimensional dark spatial soliton with vanishing transverse velocity. Single semi-infinite fractional dipole develops snake instability near the dark beam end. Depending on their phase profiles, four parallel semi-infinite fractional vortex dipoles aligned to initially form two dark stripes can evolve into two different 'cross-connects' able to branch and route probe optical beams. Perpendicular probe beam propagation in the optically-induced guiding structures is modeled and analyzed with respect to the branching efficiency to respective virtual output channels for both self-focusing and self-defocusing conditions.

Keyword list: self-defocusing, self-defocusing, Kerr nonlinearity, phase dislocation, dark beam, fractional vortex dipole, all-optical interaction, all-optical guiding.

1. INTRODUCTION

Propagation of optical beams in nonlinear media (NLM) has been a subject of continuing interest for more than four decades due to the possibility for creation of reconfigurable waveguides through the intensity-dependent refractive index change[1,2]. Such optically induced waveguides can guide weak signal beams and pulses[3,4], which motivates the investigation of novel techniques for manipulation of the transverse beam dynamics and opens possibilities for realization of waveguides with complex geometries. Besides their intriguing physical picture, particular interest in dark spatial solitons (DSSs) is motivated by their ability to induce gradient optical waveguides in bulk self-defocusing NLM[1,4-8]. Necessary but not sufficient condition for DSS formation is the self-defocusing medium nonlinearity.

The only known truly two-dimensional (2D) DSSs are the optical vortex solitons[5] whereas in one transverse spatial dimension the DSSs manifest themselves as dark stripes[9]. The odd initial condition required for generating a fundamental 1D DSS corresponds to a π-phase jump centered along the irradiance minimum of the stripe (i.e. to a step phase dislocation). The OVSs have a helical (screw-type) phase profile described by $exp(im\varphi)$ multiplier, where φ is the azimuthal coordinate and the integer number m is the so-called topological charge. 1D and 2D fundamental DSSs of these types have the common feature of zero transverse velocity with respect to the background beam if no perturbations are present. A variable number of quasi-2D dark spatial solitons of adjustable transverse velocities could be generated[10] by a proper choice of the initial phase profile (odd or even), of the width of the crossed 1D dark beams, and of the background-beam intensity.

In contrast, dark (or grey) waves are known in singular optics which slowly change their parameters, even when they are generated from perfectly odd initial conditions. Classical example are the ring dark solitary waves[11,12]. In their pioneering analysis[13] Nye and Berry conjectured that mixed edge–screw phase dislocations (fractional vortex dipoles, FVDs) cannot exist. Nonetheless, an indication of their existence was found[14] for two interacting optical vortices of opposite topological charges. Moderate saturation of the medium third-order nonlinearity enabled to suppress the snake instability of crossed 1D dark solitons and to identify 1D odd dark beams (ODBs) of finite length containing mixed-type (step-screw (SS) or edge-screw (ES)) phase dislocations[15,16]. Later on, such ODBs with SS phase dislocations were experimentally generated under controllable initial conditions by computer-generated holograms[17]. The data confirmed[17] that one can effectively control the steering dynamics of such beams by varying the magnitude and/or the length of the

1D part of the phase jump. Although two different schemes for directional coupling of signal beams by steering FVD beams were proposed in Kerr media with negative nonlinearities[18], the first successful experiment was conducted in biased photorefractive medium with a positive nonlinearity[19].

In this work we analyze numerically three different interaction schemes between ordered semi-infinite FVDs in self-defocusing and self-focusing NLM and model the branching and routing of probe beams inside the optically-induced reconfigurable interconnects. The interaction scenario modeled is 'perpendicular', i.e. the probe beams propagate perpendicular to the propagation direction of the dark beams (parallel to the dark beams itself). Within a certain interval of distances along the NLM, the inherently restless semi-infinite FVDs concatenate to form structures resembling cross-connects and further displace again thus forming effective walls of the guiding structure also in a direction parallel to the dark beam propagation. Both probe beam guiding (inside the dark structures for negative medium nonlinearity) and anti-guiding (expelling the probe beam out of the dark beam into its bright wings for positive nonlinearity) are modeled and compared with respect to the probe beam branching efficiencies into virtual output channels.

2. NUMERICAL PROCEDURE

The mixed edge-screw (ES) phase dislocation of the fractional vortex dipole (FVD) consist of an one-dimensional phase step of length $2b$, which ends, by necessity, with pairs of phase semi-spirals on π with opposite helicities. The phase profile of this ES dislocation can be described by

$$\Phi^{ES}(x,y) = \frac{\Delta\Phi}{2\pi}\left[\arctan\left(\frac{y}{x+b}\right) - \arctan\left(\frac{y}{x-b}\right)\right], \tag{1}$$

where $\Delta\Phi$ stands for the magnitude of the step portion of the dislocation and x and y denote the transverse Cartesian coordinates parallel and perpendicular to the dislocation. An increase in the ODB transverse velocity can be achieved[17] by decreasing $\Delta\Phi$, but here we refrain from exploiting this in order to keep the dark beam contrast and the refractive index modulation as high as possible. All the data in this work refer to $\Delta\Phi = \pi$. Surface plot of the ES phase dislocation is shown in Fig. 1. The slowly-varying electric field amplitude of a single FVD with ES phase dislocation is assumed to be *tanh*-shaped and, when centered on the background beam, of the form

$$E^{ES}(x,y,z=0) = \sqrt{I_0}B(x,y)\tanh\left[r_{\alpha,\beta}(x,y)/a\right]\exp\left[i\Phi^{ES}(x,y)\right]. \tag{3}$$

Here

$$r_{\alpha,\beta}(x,y) = \left[\alpha(x+\beta b)^2 + y^2\right]^{1/2} \tag{4}$$

is the effective radial coordinate and the parameters α and β are defined as follows:

$$\alpha = \begin{cases} 0 & |x| \le b \\ 1 \text{ and } \beta = -1 & \text{for } x > b \\ 1 \text{ and } \beta = 1 & \text{for } x \le -b \end{cases}. \tag{5}$$

In order to avoid any influence of the finite background beam of super-Gaussian form

$$B(x,y) = \exp\left\{-\left[(x^2+y^2)/w^2\right]^8\right\}, \tag{6}$$

its width w is chosen to exceed more that 20 times the initial dark beam width a.

The numerical simulations of the FVD propagation along the local Kerr NLM are carried out using the (2+1)-dimensional nonlinear Schrödinger equation (NLSE)

$$i\partial E/\partial(z/L_{Diff}) + (1/2)\Delta_T E - \gamma\,|E|^2\,E = 0, \tag{7}$$

which accounts for the evolution of the slowly-varying optical beam envelope amplitude E under the combined action of nonlinearity and diffraction. Here Δ_T is the transverse part of the Laplace operator, $\gamma = L_{Diff}/L_{NL}$, and $L_{Diff} = ka^2$ and $L_{NL} = 1/(k|n_2|I)$ stand for the diffraction and nonlinear length of the dark beam respectively. The minus sign in Eq. 1 means self-defocusing nonlinearity (necessary conditions for dark spatial soliton formation and for waveguiding by dark beams). In the above notations, k is the wave number inside the medium and I is the peak field intensity. The transverse spatial coordinates (x and y) are normalized to the ODB width a. The model NLSE we solved numerically by means of the split-step Fourier method with a computational window spanning over 1024x1024 grid points. As a standard test we modeled the formation of a fundamental 1D dark spatial soliton and compared it to the diffraction-compensated dark

beam formed by a quasi-infinite FVD (dipole much longer than the background beam; $2b >> w$). It is worth mentioning that the vanishing transverse velocity of this quasi-infinite self-supported FVD dark beam makes it indistinguishable from the exact 1D dark spatial soliton. In the following simulations the background beam intensity is kept equal to that needed to form a fundamental 1D DSS of "infinite" length ($I = I_{sol}^{1D}$, i.e. $\gamma = 1$).

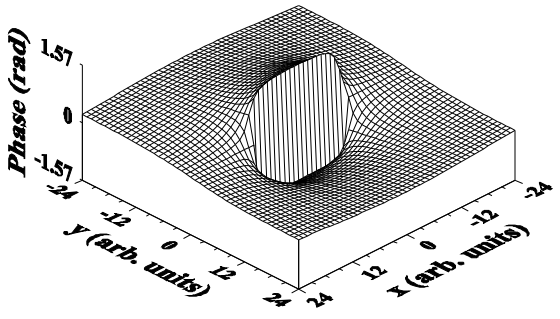

Fig. 1 Edge-screw mixed phase dislocation (fractional vortex dipole, FVD) described by Eq. 1.

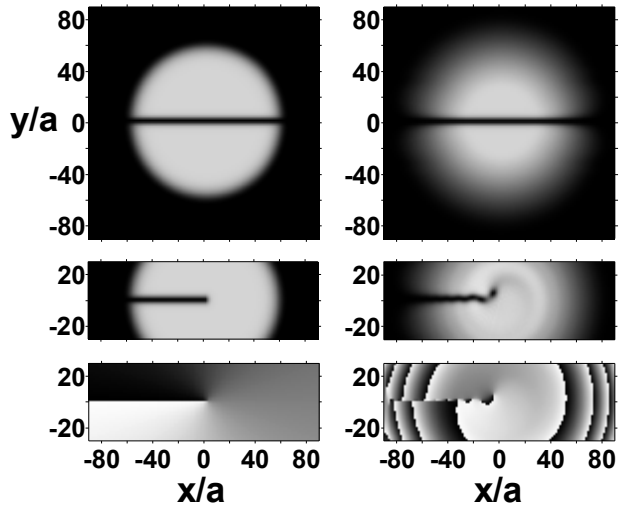

Fig. 2 Upper row - Power density distributions of an infinite FVD beam at the entrance of the NLM (left) and at a nonlinear propagation distance z/L_{Diff}=6 (right). Middle and bottom row – Power density and phase distributions of a semi-infinite FVD beam at the same distances.

3. EVOLUTION OF THE FRACTIONAL VORTEX DIPOLES

As shown in previous analyses of ODBs with mixed SS dislocations[17,18], the background-beam intensity has a weak influence on the dark beam steering. Negative nonlinearity is important, however, for keeping the optically induced refractive index modulation (e.g. dark beam profile and refractive index profile) steep, which is crucial for all-optical guiding, deflection, and switching of signal beams or pulses. Because, generally, the finite-length ODBs with mixed phase dislocations shorten and flatten along the self-defocusing nonlinear media (tending asymptotically to washout), the power density redistribution on the background creates peaks near the ODBs (behind them, with respect to the propagation direction). The self-defocusing nonlinearity tends to suppress their growth and contributes, as the diffraction does, to their broadening[20]. In a self-focusing Kerr nonlinear media, however, the peaks near the ODBs can initiate filamentation of the background beam for which geometry-controlled conditions for their intensity ratio and offset are found[20]. When the length $2b$ of the FVD beam is much larger than the background beam diameter (and the computational window) and it ends in the center of the background, this FVD beam we will denote as "semi-infinite". In the upper row in Fig. 2 we show the power density distribution of a quasi-infinite FVD beam at the entrance of the NLM and at z/L_{NL}=6 for $I = I_{sol}^{1D}$. In the second row we show the input (left) and output power density distribution (right frame) of a semi-infinite FVD at the same nonlinear propagation distance. As seen, the semi-infinite FVD beam develops snake instability[21] and one vortex becomes clearly detached from the bending rest of the dark beam. The closer inspection of the respective phase profile (bottom right frame in Fig. 2) shows that four vortices with alternating topological charges are formed, three of them with highly overlapping cores.

As a next step let us consider the structure and the evolution of two inline FVDs. In order to get higher modulation depth in the interaction region near the center of the background, we shifted the ends of the FVD beams from its center to overlap in a region of length $\Delta = 2.6a$. The two characteristic cases are shown in Fig. 3 – opposite (left column) and equal phase semi-helicities (right). In both cases the overlapping of the FVD beams causes larger modulation in the center as compared to this in the remaining part of the composite dark beam. This excess "lack of energy" is emitted as dispersive waves perpendicular to the FVD beams. In the case of opposite helicities (Fig. 3, left column) in the overlapping region the phase distribution resembles this of a mixed phase dislocation of limited length and, as characteristic for beams with such dislocations, they steer in transverse direction. (Here this steering looks like

dark stripe bending only.) In the second case of FVDs with opposite helicities (Fig. 3, right column) the ends of the semi-infinite beams steer in opposite directions and evolve like almost independent semi-infinite FVD (see the bottom right frames in Fig. 2).

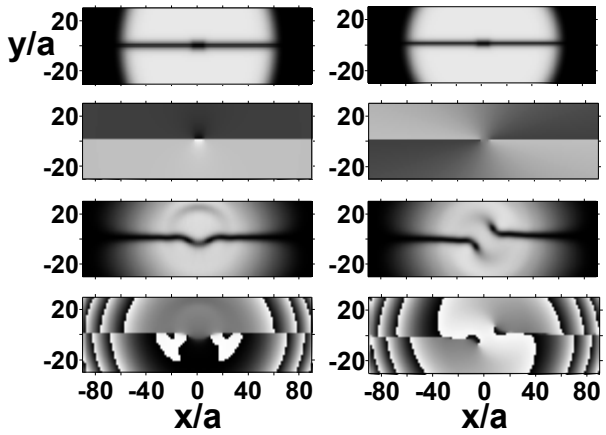

Fig. 3 Power density (odd rows) and phase distributions (even rows) of pairs of overlapping ($\Delta = 2.6a$) inline semi-infinite FVD beams in the case of *opposite* (left column) and *equal* helicities (right column) of the phase semi-spirals. Top two rows – z=0, bottom two rows – at the exit of the NLM (z/L_{Diff}=6).

Let us further concentrate on the following three possible cases:

Case A: Pair of two parallel one-dimensional dark beams with pure one-dimensional phase dislocations on π. The larger dark beam width in their central parts is kept (for consistency, not by necessity) identical to these in cases B) and C) where it is a result of an intentional overlapping of the FVD beams.

Case B: Pair of two inline semi-infinite FVD beams for which the overlapping FVDs have *opposite* helicities, whereas the two pairs have *opposite* phase distributions.

Case C: Pair of two inline FVD beams for which the overlapping semi-infinite FVDs have *equal* helicities, whereas the two pairs of semi-infinite FVDs have phase distributions with the *same* gradients.

In all three cases the length of the FVD beam's overlap near the background beam center is $\Delta = \pm 1.3a$ and the vertical offset from the background beam diameter is $\Delta y = \pm 1.8a$. Although the amplitude distributions in all three cases are identical (Fig. 4, second row), they entirely different phase profiles (Fig. 4, first row) rule their disparate transverse dynamics along the self-defocusing NLM. It is worth mentioning that when two *identical* semi-infinite FVDs are aligned inline (no difference overlapping or not) the neighboring phase semi-spirals have *opposite* helicities. The phase profile of a single FVD beam of limited length ends also by semi-spirals with opposite helicities (see Fig. 1). Since the steering direction is phase-dependent[17,18] the FVD beam overlapping does not alter it.

In Case A we simply have propagation and interaction (repulsion in a local NLM[22,23]) of closely-spaced one-dimensional dark spatial solitons. The modulation in the middle of these beams leads to emission of a dispersive wave serving as a perturbation (Fig. 4, left column, z=3L_{NL}). As a result, the dark beams slightly bend but do not develop snake instability and do not decay into single vortices up to z=6L_{NL} (Fig. 4, left column). For probe signals entering the defocusing NLM perpendicularly to the background beam, the optically-induced waveguiding structure in this case consists essentially of two parallel planar waveguides.

In Case B, because of the specific orientation of the phase profiles of the FVD beams, the central parts of the dark beams bend inwards and overlap, thus forming a cross-connect-like structure at z=3L_{NL}. With increasing the nonlinear propagation path length up to z=6L_{NL} the beams in this region repel, bend, split and decay into four (sill highly overlapping) optical vortices. Hence, the proper position for the probe beam to enter perpendicularly the defocusing NLM would be at z=3L_{NL}. The effective waveguide structure it will see will be this of a symmetric X-junction (input inline with one of the outputs).

The effective waveguiding structure for perpendicularly propagating probe beams shown in Case C resembles bent planar waveguides. If the probe beam enters the defocusing NLM perpendicularly at z=1L_{NL} it will see upper left planar waveguide merging into the lower right waveguide. At smaller and longer propagation distances the connection

between the FVDs (and the effective waveguide) becomes broken. Qualitatively, in Case C the four FVD beams evolve more or less independently. Of course, because of the inherent dynamics of the FVD beams, the probe beam guiding efficiencies could not be expected to be 100% and in cases B and C one can expect certain (different) branching ratios for the incoming signal beams. Moreover, in the transverse pump-probe geometry the effective nonlinear interaction length extends over the pump beam cross section only.

The above comments for cases A, B, and C are correct for pump self-defocusing and pump-induced defocusing Kerr nonlinearity ensuring probe beam guiding inside the dark beam cores. Further we will consider also the anti-guiding case, for which the nonlinearity for pump-induced probe beam spatial phase modulation is positive, whereas the nonlinearity for pump self-phase modulation in space is negative (pump self-defocusing condition). This situation can be realized in a nonlinear medium with orientational Kerr nonlinearity by choosing the probe beam polarization to be perpendicular to this of the pump beam. Since in this case the evolution of the dark waveguides remains unchanged, the perpendicularly propagating probe beams with crossed polarization become split and expelled out from the dark beams, thus becoming anti-guided by the dark beams and guided by the bright wings of the FVD beams.

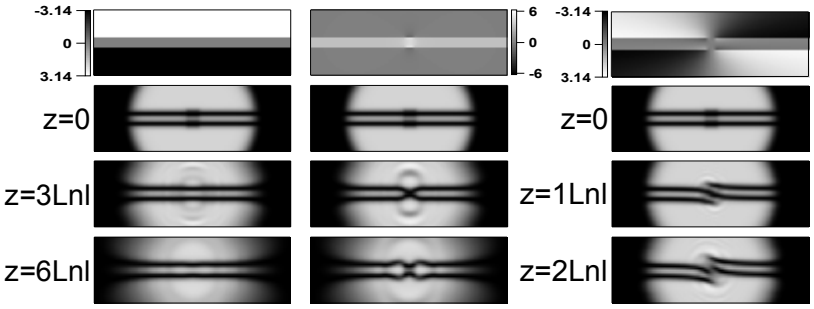

Fig. 4 Phase profiles (upper row) and power density distributions of pairs of inline semi-infinite and overlapping FVDs at the entrance of the NLM and at distances $z=3L_{NL}$ and $6L_{NL}$ for case A and case B and at $z=1L_{NL}$ and $2L_{NL}$ for case C.

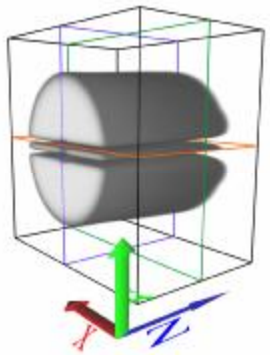

Fig. 5 Scheme of the background beam carrying the FVD beams inside the NLM. Perpendicular propagation - along the *x*-axis. The tiny (color) lines cross in the *yz*-plane approximately at the position where the probe beams enter the NLM.

In Fig. 5 we show schematic view of the NLM with notation of the coordinate system axes. Perpendicular propagation takes place along the *x*-axis. The horizontal and vertical tiny lines cross in the yz-plane approximately at the position where the probe beams enter the NLM. For clarity, the embedded image corresponds to the simulation in Case A (see Fig. 4).

4. BRANCHING OF PROBE BEAMS INSIDE THE OPTICALLY-INDUCED GUIDING STRUCTURES

The incoming probe beams are modeled to be Gaussian and of widths, equal to the vertical extent of the one-dimensional dark soliton shown in Fig. 2. If one thinks that the cell containing the NLM is parallelipiped (see Fig. 5), its depth (along the z-axis) extends to $6L_{NL}$ in cases A and B, and up to $2L_{NL}$ in case C. When the probe beams enters the NLM perpendicularly, it evolves along the propagation coordinate *x* diffracting and experiencing the refractive index modulation mainly in the *yz*-plane due to the background beam with the nested FVD beams. This is modeled by solving the equation

$$i\partial S/\partial x + [1/(2L_{DS})](\partial^2/\partial y^2 + \partial^2/\partial z^2)S - |E|^2 S/L_{NL} = 0 \ . \qquad (8)$$

Here $L_{DS} = k_S a_S^2$ is the diffraction length of the bright probe beam of width a_S and $L_{DS} = L_{Diff} = L_{NL}$. Since the evolution of the ordered FVDs is followed up to $z=6L_{NL}$ for cases A and B and up to $2L_{NL}$ in case C and from each simulation for the pump beams we stored 256 *E*-field amplitude and phase distributions, the computational grid for the probe beams spans over 256x256 grid points. Each probe beam enters well centered (in the *yz*-plane) the induced waveguides at

location $z=3L_{NL}$ for cases A and B and at $z=1L_{NL}$ for case C. The minus sign in Eq. 8 means induced-defocusing regime and probe beam guiding, whereas the anti-guiding regime is modeled by reversing the sign to plus.

4.1. Perpendicular probe beam propagation in a guiding regime

The results for this case are shown in Fig. 6 and in Table 1. The presence of strong refractive-index gradients along the *y*-axis for $I = I_{SOL}^{1D}$ improves the linearly redistributed signal (see Fig. 6, case L) to channels 1 and 2 from 44%/20% to 72%/18% when channel 1 is initially addressed (see Table 1). When the probe beams is entering initially channel 2, the (inverted) proportionality is quite similar. By changing the phase profiles of the pairs of overlapping pump FVD beams the cited 72% guiding efficiency when input channel 1 is addressed, can be changed to 66% (case B) and to 61% (case C). Qualitatively the same is the tendency when input channel 2 is initially addressed. We performed also separate sets of simulations for twice higher background beam intensity ($I = 2I_{SOL}^{1D}$). In this way the branching ratios can be changed from e.g. 72%/18% to 82%/14% in case A and from 66%/25% to 69%/21% in case B when initially channel 1 is addressed only.

As seen from Table 1, the general tendency in cases A and B is that the increase of the background-beam intensity leads to deeper modulation of the refractive index in the straight parts of the waveguides and to a somewhat weaker probe beam branching in the interaction region. Because in case C, in the zone of propagation of the probe wave, one optically-induced waveguide becomes coupled to another one whereas the other two become decoupled only (Fig. 4, right column, $z=L_{diff}$), the higher intensity leads to a weak increase of the coupling efficiency into one of the channels and to a decrease of this efficiency into the other channel.

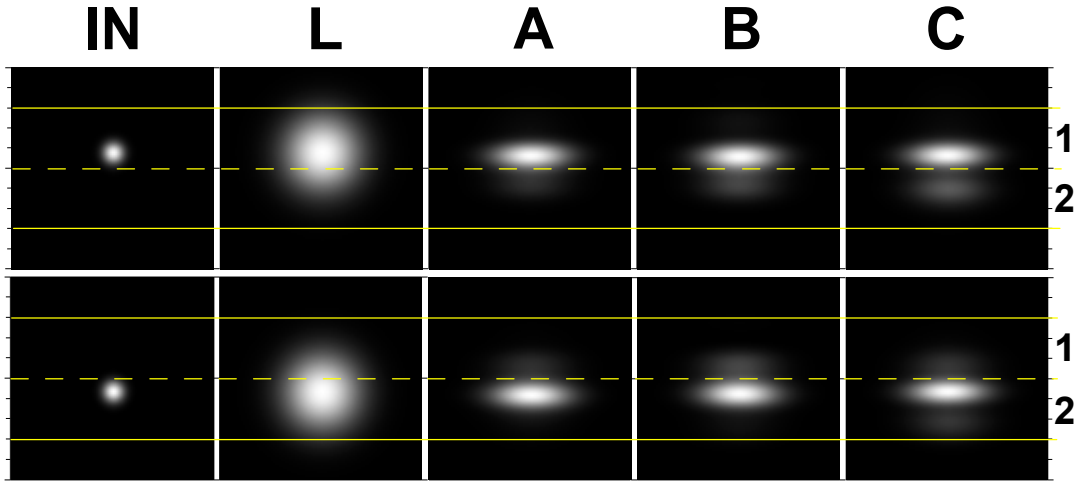

Fig. 6 Probe beams in guiding regime: Input probe beams (IN) entering the NLM perpendicularly to the pump, in the center of the imaginary cell containing the NLM (Fig. 5) and propagating along the x-axis. (L): Output power density distributions of the probe beams propagating linearly to the exit of the cell (x/L_{diff}=3.5). The results for the probe beams at the exit of the NLM in the nonlinear regimes for cases A, B, and C are correspondingly denoted. $I = I_{SOL}^{1D}$. The horizontal dashed yellow line indicates the *xz* input symmetry plane, whereas the solid lines denote the virtual output channels for which the probe-beam branching efficiencies are summarized in Table 1.

Table 1. Perpendicular pump and probe beams in guiding regime: Probe beam branching efficiencies in the different cases; (L)-linear; (A), (B), and (C) – nonlinear propagation regimes for cases A, B, and C, respectively. (IN)-input.

	Channel	IN	L	A	B	C
$I = I_{SOL}^{1D}$	**1**	100%	44%	72%	66%	61%
	2	0%	20%	18%	25%	25%
	1	0%	20%	19%	24%	20%
	2	100%	44%	68%	63%	58%

4.2. Perpendicular probe beam propagation in an anti-guiding regime

The results for this case are shown in Fig. 7 and in Table 2. Both composed picture and table show that the anti-guiding nature of the process strongly dominates the fine effects caused by the differences in the dark beam structure. In Fig. 7 one can clearly see that the probe beam is split in two sub-beams separated by a dark beam with a flat phase (i.e. not by a singular beam as in the case of the $TEM_{01,10}$ laser cavity mode). The largest difference in the (anti-)guiding efficiencies 58%/40% was estimated in case C for the signal entering on-axially the upper dark beam. For the same probe beam but in case B, within the 1% accuracy in calculating the efficiencies, we estimate equal sub-beam energies. In view of the results from this sub-section one can conclude that probably the most simple structure ensuring well pronounced anti-guiding of probe beams could be just a single fundamental dark spatial soliton.

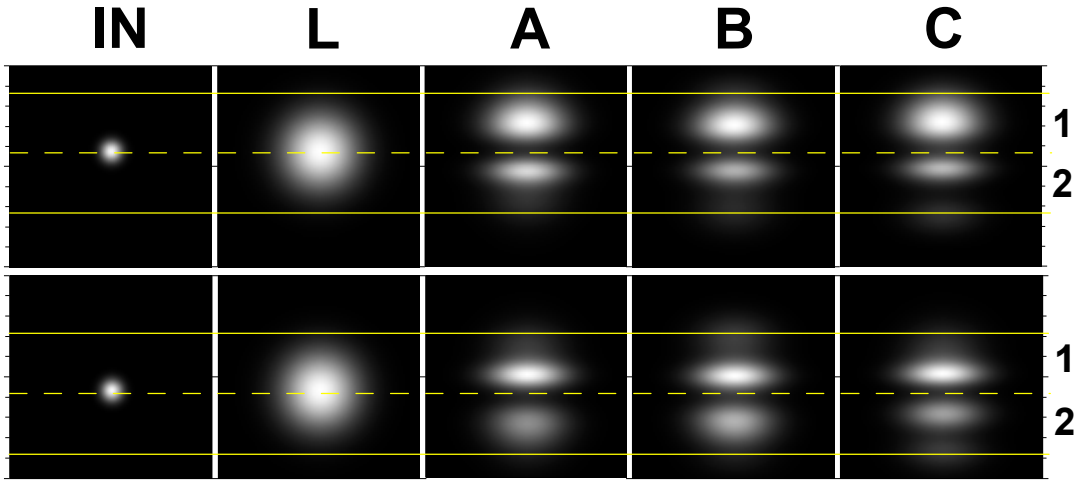

Fig. 7 Probe beams in anti-guiding regime: Input probe beams (IN) entering the NLM perpendicularly to the pump, in the center of the imaginary cell containing the NLM (Fig. 5) and propagating along the *x*-axis. (L): Output power density distributions of the probe beams propagating linearly to the exit of the cell (x/L_{diff}=3.5). The results for the probe beams at the exit of the NLM in the nonlinear regimes for cases A, B, and C are correspondingly denoted. $I = I_{SOL}^{1D}$. The horizontal dashed yellow line indicates the *xz* input symmetry plane, whereas the solid lines denote the virtual output channels for which the probe-beam branching efficiencies are summarized in Table 2.

Table 2. Perpendicular pump and probe beams in anti-guiding regime: Probe beam branching efficiencies in the different cases; (L)-linear; (A), (B), and (C) – nonlinear propagation regimes for cases A, B, and C, respectively. (IN)-input.

	Channel	IN	L	A	B	C
$I = I_{SOL}^{1D}$	**1**	50%	50%	55%	49%	58%
	2	50%	50%	44%	49%	40%
	1	50%	50%	56%	56%	55%
	2	50%	50%	43%	43%	44%

5. CONCLUSION

The presence and evolution of ordered structures of odd dark beams of semi-infinite length carrying edge-screw phase dislocations (fractional vortex dipoles, FVDs) is studied in a self-defocusing Kerr nonlinear medium. We found appropriate conditions to control the process of crossing the dark beams in a way suitable for probe-beam cross-switching. For this purpose we essentially use the numerically proven features of the FVDs that a quasi-infinite vortex dipole (dipole much longer than the background beam) evolves in one-dimensional dark spatial soliton and that a single semi-infinite fractional dipole develops snake instability near the dark beam end. Depending on their phase profiles, four parallel semi-infinite fractional vortex dipoles aligned to initially form two dark stripes can evolve into two different cross-connects able, in the guiding regime, to partially redirect perpendicularly-propagating probe optical beams at different branching efficiencies. In the anti-guiding regime of the probe waves, however, the anti-guiding nature of the process strongly dominates the fine effects caused by the differences in the dark beam structure and the differences in the

efficiencies in the virtual output channels in the anti-guiding regime are relatively low. Being still far from discussing particular practical applications, the desirable high-efficient routing of probe beams by fractional vortex dipoles in the guiding regime seems feasible provided the interaction length in the overlapping region of the dipoles becomes longer. In the anti-guiding regime probably the most simple structure ensuring well pronounced probe beam splitting is just a single fundamental dark spatial soliton. The presented results provide reasonable first step for further optimization of FVD-based probe beam guiding and branching schemes in the guiding regime.

6. ACKNOWLEDGMENTS

This work was supported by the NSF-Bulgaria (grants DO-02-0114/2008 and DRNF-02-8/2009), and by the DFG in the framework of Forschergruppe 532 "Nichtlineare raum-zeitliche Dynamik in dissipativen und diskreten optischen Systemen".

7. REFERENCES

[1] Stegeman, G. I. and Segev, M., "Optical spatial solitons and their interactions: Universality and diversity," Science **286**, 1518–1523 (1999).
[2] Kivshar, Yu. S. and Luther-Davies, B., ''Dark optical solitons: physics and applications," Phys. Rep. **298**, 81–197 (1998).
[3] De La Fuente, R., Barthelemy, A. and Froehly, C., "Spatial-soliton-induced guided waves in a homogeneous nonlinear Kerr medium," Opt. Lett. **16**, 793–795 (1991).
[4] Snyder, A. W. and Sheppard, A. P., "Collisions, steering, and guidance with spatial solitons," Opt. Lett. **18**, 482–484 (1993).
[5] Swartzlander, Jr., G. and Law, C., ''Optical vortex solitons observed in Kerr nonlinear medium,'' Phys. Rev. Lett. **69**, 2503–2506 (1992).
[6] Ostrovskaya, E. A. and Kivshar, Yu. S., ''Nonlinear theory of soliton-induced waveguides,'' Opt. Lett. **23**, 1268–1270 (1998).
[7] Carlsson, A. H., Malmberg, J. N., Ostrovskaya, E. A., Alexander, T. J., Anderson, D., Lisak, M. and Kivshar, Yu., ''Linear and nonlinear waveguides induced by optical vortex solitons,'' Opt. Lett. **25**, 660–662 (2000).
[8] Law, C. , Zhang, X. and Swartzlander, Jr., G., ''Waveguiding properties of optical vortex solitons,'' Opt. Lett. **25**, 55–57 (2000).
[9] Allan, G., Skinner, S., Andersen, D. and Smirl, A., ''Observation of fundamental dark spatial solitons in semiconductors using picosecond pulses,'' Opt. Lett. **16**, 156–158 (1991).
[10] Neshev, D, Dreischuh, A., Dinev, S. and Windholz, L., ''Controllable branching of optical beams by quasi-two-dimensional dark spatial solitons,' J. Opt. Soc. Am. B **14**, 2869–2876 (1997).
[11] Kivshar, Yu. S. and Yang, X., ''Ring dark solitons,'' Phys. Rev. E **50**, R40–R43 (1994); ''Dynamics of dark solitons,'' Chaos, Solitons Fractals **4**, 1745–1758 (1994).
[12] Neshev, D., Dreischuh, A., Kamenov, V., Stefanov, I., Dinev, S., Fliesser, W. and Windholz, L., ''Generation and intrinsic dynamics of ring dark solitary waves,'' Appl. Phys. B **64**, 429–433 (1997); Dreischuh, A., Neshev, D., Paulus, G. G., Grasbon, F. and Walther, H., "Ring dark solitary waves: Experiment versus theory," Phys. Rev. E **66**, art. 066611 (1-7) (2002).
[13] Nye, J. F. and Berry, M. V., ''Dislocations in wave trains,'' Proc. R. Soc. London, Ser. A **336**, 165–190 (1974).
[14] Bazhenov, V., Soskin, M. and Vasnetsov, M., ''Screw dislocations in light wavefronts,'' J. Mod. Opt. **39**, 985–990 (1992); Basistiy, I., Bazhenov, V., Soskin, M. and Vasnetsov, M., ''Optics of light beams with screw dislocations,'' Opt. Commun. **103**, 422–428 (1993).
[15] Dreischuh, A., Paulus, G. G. and Zacher, F., ''Quasi-2D dark spatial solitons and generation of mixed phase dislocations,'' Appl. Phys. B **69**, 107–111 (1999).
[16] Dreischuh, A., Paulus, G. G., Zacher, F. and Velchev, I., ''Steering one-dimensional odd dark beams of finite length,'' Appl. Phys. B **69**, 113–117 (1999).
[17] Dreischuh, A., Neshev, D., Paulus, G. G. and Walther, H., "Experimental generation of steering odd dark beams of finite length," J. Opt. Soc. Am. B **17**, 2011–2016 (2000).
[18] Neshev, D., Dreischuh, A., Paulus, G. G. and Walther, H., "Directional coupling of optical signals by odd dark beams with mixed phase dislocations," Appl. Phys. B **72**, 849–854 (2001).
[19] Maleshkov, G., Neshev, D. N. and Dreischuh, A., "Nonlinear beam steering by fractional vortex dipoles," Phys. Rev. A. **80**, art. 053828 (1-5) (2009).
[20] Maleshkov, G., Hansinger, P., Dreischuh, A., and Paulus, G. G., "Fractional vortex dipoles of edge-screw type in self-focusing Kerr nonlinear media," *Proc. SPIE* **7747**, art. 77471P (2011).
[21] V. Tikhonenko, J. Christou, B. Luther-Davies, and Yu. S. Kivshar, ''Observation of vortex solitons created by the instability of dark soliton stripes,'' Opt. Lett. **21**, 1129–1131 (1996).
[22] K.J. Blow and N.J. Doran, "Multiple dark soliton solutions of the nonlinear Schrödinger equation," Phys. Lett. A **107**, 55–58 (1985).
[23] A. Dreischuh, D. N. Neshev, D. E. Petersen, O. Bang, and W. Krolikowski, "Observation of attraction between dark solitons," Phys. Rev. Lett. **96**, art. 043901 (2006).